Electronic design for a bleeding detector to be used in intraoperative radiotherapy applications

R. García-Gil, S. Casans, E. Sanchis-Sánchez, I. Pérez-Calatayud, J. Pérez-Calatayud, E. Sanchis, *Senior Member, IEEE*

Abstract— **An electronic design for a bleeding detector used with mobile linac during intraoperative radiotherapy (IORT) is presented. It consists on a readout circuit based on a De Sauty Bridge and a wireless power supply using a supercapacitor. The goal is the measurement of the height of fluid present in the applicator in order to avoid a misadministration dose during the irradiation process. A minimum measurement height of 5 mm is required by clinic to be confident with the selected radiation dose. The measurement circuit uses a capacitive sensor which detects variations lower than 0.1 pF. The readout circuit converts dynamic capacitance variation from the bleeding detector into an analog voltage signal. Tests have been performed with a 40 mm diameter polymethyl methacrylate applicator (PMMA) using water. Non-bevelled PMMA 0º and 45º tilted have been considered, being this the worst condition used in the clinic. The actual height of the fluid with respect to that measured by our system shows good linearity and repeatability within acceptable limits. For 0º tilted, a 2 mm height fluid detection is achieved well below the 5 mm height demanded by clinic. For 45º tilted, a 5 mm height fluid detection is achieved.**

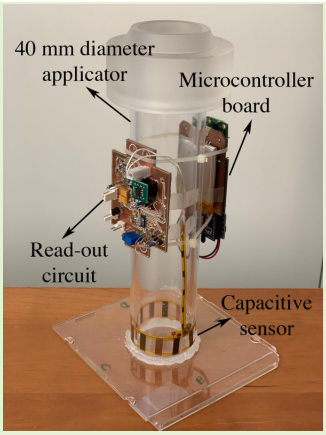

***Index Terms*—Intraoperative radiotherapy, mobile linacs, bleeding detector, capacitive sensor, De Sauty bridge, wireless supply.**

I. Introduction

RADIATION ONCOLOGY or Radiotherapy (RT) is a clinical modality that uses ionizing radiation for the treatment of oncologic lesions and some other minor benign ones [1]. The aim of RT is to deliver sufficient dose to control the disease whereas keeping it as low as possible, both in normal tissue and in surrounding organs at risk.

One specific RT modality is the intraoperative radiotherapy (IORT). It is applied during the patient's surgery once the lesion has been totally or partially removed. The aim of the IORT is to neutralize potential remaining cells or gross disease by irradiating the tumour bed.

Intraoperative radiation electron radiotherapy (IOERT) is based on electrons beam with a set of energies covering typically the range of 6 to 12 MeV and then being able to treat lesions up to 35-40 mm depth. The collimation of the beam into the clinically required fields is achieved by means of applicators, the size of which depend on the volume of the lesion to be treated [2]. IOERT is a well-established modality that is currently gaining popularity and being applied to a wide variety of specific diseases [2], [3].

In this technique, one of the uncertainties or dose misadministration events is the potential bleeding in the post-resected surface [3], that can be especially critical in high-vascularized scenarios or in presence of organic fluids. In fact, it was evidenced in the in vivo experimental study of López-Tarjuelo et al. [4] in which they faced with significant deviations due to the blood presence. We ourselves have faced with very vascularized scenarios so frequent suction was required to keep it free of fluids along the irradiation procedure.

To assure that the irradiation has been carried out in a foreseen manner, avoiding serious errors due to variations in the irradiation depth produced by the presence of fluids, a bleeding

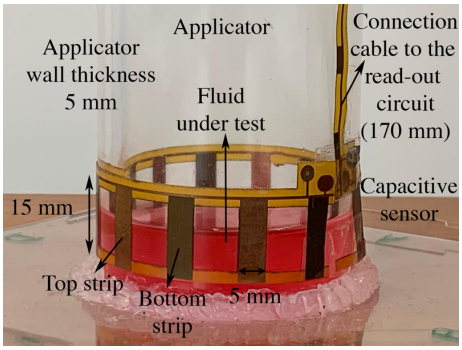

Fig. 1. Capacitive sensor located at the bottom part of the applicator with fluid inside.

[2]020-09-19

R. Garcia-Gil (rafael.garcia@uv.es), S. Casans (silvia.casans@uv.es), I. Pérez-Calatayud (pecaig@alumni.uv.es) and E. Sanchis (enrique.sanchis@uv.es) are with Department of Electronic Enginnering, University of Valencia, E-46111 Spain.

E. Sanchis-Sánchez (enrique.sanchis-sanchez@uv.es) is with Department of Physical Therapy, University of Valencia, 46010 Spain

J. Pérez-Calatayud (perez_jos@gva.es) is with Department of Radiation Oncology, La Fe Polytechnic and University Hospital, Valencia, E-46026, Spain.

detection into the applicator during IOERT can be very useful. To guarantee a correct administration of the dose, it must be ensured that the fluid present in the applicator is less than 5 mm high [4] in the range 3-12 mm height.

According to the clinical procedure used in IOERT sessions, the detector must not be in contact with the tissue and therefore must be embedded in the applicator. The applicator is sterilized in each session so that its contact with the patient's tissue is clinically guaranteed. The use of capacitive sensors with electrodes placed on the outer side of the applicator are suitable for this application.

A capacitive based bleeding detector was proposed by Sanchis et al. [5], [6] for polymethyl methacrylate applicators (PMMA). The use of PMMA applicators has the advantage of being transparent compared to other metallic applicators [7]. Applicators have diameters ranging from 30 to 120 mm with bevel angles ranging from 0° to 45°, wall thickness is 5 mm.

The sensor geometry used in [5], [6] is based on two capacitive plates, each one formed by a set of strips (Fig. 1). The strips of each plate are interspersed with each other in such a way that it reduces the effects of the asymmetry in the distribution of the fluid to be detected regardless the different orientations of the applicators used when it is tilted. Besides, it allows the surgeon to have a high lateral visibility through the applicator.

Sanchis et al. [6] have observed a fringing effect in the physical boundaries of the sensor. For this reason, a sensor height of 15 mm has been selected, large enough for the required dynamic range (3-12 mm).

Although capacitive fluid level detectors have been widely analysed [8]–[12], the special geometry of the used capacitive sensor together with the separation between the detector and the fluid (5 mm thickness of the applicator) and the minimum detection height requirements imposed by clinic (5 mm) are the bases of the challenge of this work.

The goal of this work is to present the electronic design and evaluate the result of the bleeding detector read-out used in [5], [6] for its application in IOERT. The work has focused on the measurement circuit and its supply since the proposed sensor geometry has been widely analyzed in the aforementioned references.

For the selected bleeding detector very low-level capacitance variations have to be measured. For this purpose, different approaches are found in the literature [13]–[19]: the charge balancing, the AC bridge and the LC oscillator. The charge balancing method introduces errors both because the very high amplifier input impedance needed and the required switch for the charging-discharging process [14]. The LC-based solution is suitable as it offers good immunity to noise and EMI [14]. However, in our application we have chosen the AC bridge solution for simplicity during the implementation and development of the prototype since we do not have a particularly severe EMI scenario.

The measurement circuit consists of an AC-based De-Sauty Wheatstone bridge circuit [12], [20]–[22] with rectification and filtering. Due to the very low-level capacitance variation (less than 0.1 pF), a two-stage amplification has been employed. In view of a future industrialization, a wireless power supply with supercapacitor-based storage [23], [24] has been designed. This

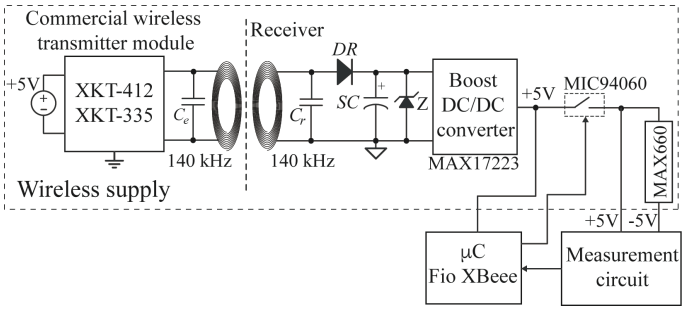

Fig. 2. Block diagram of the proposed measurement system.

will allow to finally embed all the circuitry in the applicator itself, with no external contact, for a proper applicator sterilization as required by the clinic.

A prototype has been developed whose validity has been carried out for 40 mm diameter non-bevelled applicator 0º and 45º tilted.

II. Electronic Circuit

Fig. 2 shows the block diagram of the implemented bleeding detection system. In order that the entire circuit can finally be embedded in the applicator itself, the following considerations have been taken into account:

- Components of reduced size and low consumption have been selected.

- A wireless power supply with supercapacitor-based storage (SC in Fig. 1) has been included, which ensures the minimum autonomy required by the clinic (i.e. 30 minutes).

- For a low-power consumption, a conditioning stage for disconnecting the measurement system has been incorporated. Also, the microcontroller will remain in sleep mode until data collection begins.

The main blocks are described below.

A. Wireless Power Supply

The Wireless Power Supply circuit is shown in Fig. 2. A transmitting antenna (located outside the applicator) has been designed so that they will be imbricated in the upper part of the applicator. A similar transmitting antenna, located outside the applicator, has been designed in order to obtain maximum coupling between them. As no size constraint exists for the transmitting stage, a commercial module has been selected. The 5V/2A wireless charger module from Shenzhen Core Ketai Electronics Co., Ltd. has been used, in which the turns of the emitting antenna have been modified. It can produce a maximum current of 1 A with a transmission distance up to 10 mm. According to the new transmission antenna, the C_e capacitor has been modified to fix the desired resonance frequency (140 kHz).

The spirals that form the receiving antenna will be embedded in the upper part of the applicator so the reception stage has been designed to minimize its size. It is formed by the receiving antenna and the C_r capacitor to set the same resonance frequency as in the emitting stage. Once this signal has been rectified (*DR* diode) it is used to charge the *SC*. The SC has been dimensioned so that it has an autonomy greater

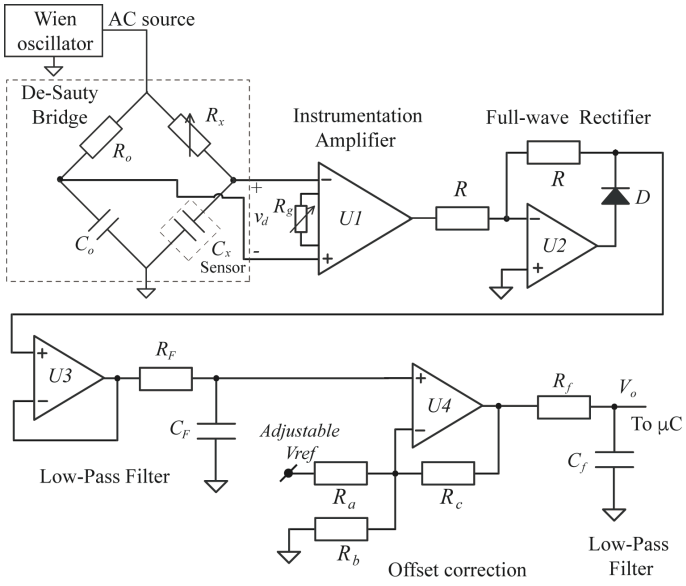

Fig. 3. Conditioning circuit for the capacitive sensor.

than 30 minutes (typically required by the clinic) for an estimated consumption of 50 mA. A 4.2 V SC from the Vishay BCcomponents family 196 HVC ENYCAPTM has been selected. The dimension of the selected SC allows to be embedded it in the applicator. In order not to exceed this voltage a 3.9 V zener diode (*Z*) has been placed in parallel.

A step-up regulator is required to obtain the 5 V necessary to supply the conditioning circuitry from the unregulated voltage of the *SC*. We have used the ultra-low quiescent current boost DC-DC converter MAX17223 which allows a 5 V regulated output voltage for an input voltage range between 0.95-5.5 V.

According to the selected *SC* and the boost regulator, the power supply will be guaranteed for a voltage variation in the *SC* from 0.95-4.2 V (ΔV_{sc} = 3.25 V). Taking into account a minimum autonomy of 30 min (t_{aut}) and an estimated current consumption of 50 mA we will need a capacitor value:

$$SC > \frac{I_c \cdot t_{aut}}{\Delta V_{sc}} = 27.7\ F. \quad (1)$$

A 90 F SC has been selected which meets the minimum required autonomy.

In addition to the regulated 5 V output, the conditioning board supply requires -5 V which is generated with the 5 V voltage using the MAX660 IC (Fig. 2).

The MIC94060YC6-TR switch allows the connection of the power supply to the conditioning board only when data collection begins. The microcontroller is permanently connected to power but in sleep mode until data collection begins.

B. Read-out circuit

In order to measure the very small capacitance variation of the proposed level transducer (in the range of 0.1 pF), an AC-based De-Sauty bridge circuit [12], [20] has been employed, as shown in Fig. 3. The AC source is generated by means of a Wien bridge oscillator designed at a stable frequency f = 20 kHz using the AD8627 low-power operational amplifier (OA). The De-Sauty bridge is formed of a reference resistor and capacitance (R_o, C_o), the capacitor sensor (C_x) and a potentiometer (R_x) for bridge balancing.

The value of C_o is taken close to the value of C_x when no fluid exists in the applicator (zero condition $C_x(0) \equiv C_1 \approx C_o$), R_o has been taken so that the cutoff frequency f_c of the voltage divider R_o-C_o is below the frequency of the AC source,

$$f_c = \frac{1}{2\pi R_o \cdot C_o} < 20\ kHz. \quad (2)$$

To determine the value of C_o, we have measured the capacity of the sensor at 20 kHz during the zero condition (C_1) using the impedance analyzer E5061B from Agilent, obtaining a value of C_1 = 95.8 pF. With this measure, a value C_o = 100 pF has been selected. In this way, according to (2), R_o = 100 kΩ has been taken.

Assuming $C_x = C_1 + \Delta C$, with ΔC very small ($2\pi f R_x \Delta C \ll 1$), and the bridge balanced ($R_o \cdot C_o = R_x \cdot C_1$), the output voltage v_d has a linear dependency with ΔC:

$$v_d \approx \frac{j2\pi f R_x}{(j2\pi f C_o R_o + 1)^2} \cdot \Delta C \quad (3)$$

Because the capacitance change ΔC is very small (less than 0.1 pF) a large amplification is necessary. The programmable gain instrumentation amplifier (IA) AD8221 with 100 dB CMRR has been used for a first amplification, as shown in Fig. 3. We have selected a gain of 50.4 (R_g = 1 kΩ).

The IA output is then rectified (*R-U2-D*) and filtered (R_F, C_F) to obtain a DC voltage which is proportional to the measurement value. Cut-off frequency has been fixed to 10 Hz ($\ll f$). An accurate full-wave rectifier based on OA (*U2*) and diode (*D*) has been used.

Due to the parasitic effect, the balance of the bridge could not be perfectly achieved which means that there is always a DC component in the output signal from the bridge. In fact, a slight bridge unbalance is necessary for the full-wave rectifier to perform properly. This is the reason why this DC component has not been previously eliminated by means of the IA (*U1* in

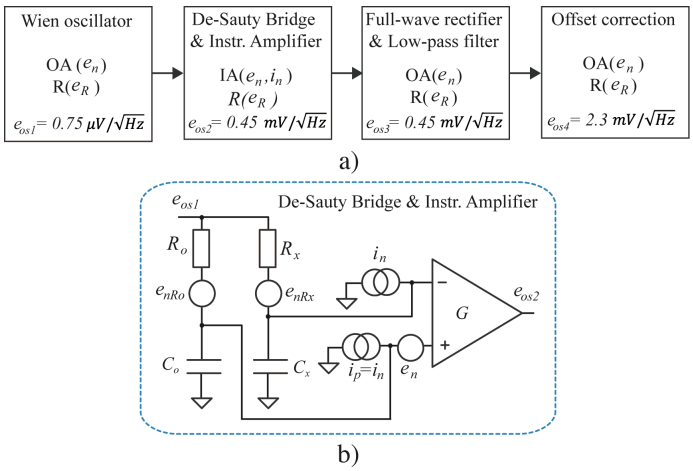

Fig. 4. Circuital model for noise analysis.

Fig. 3). Therefore, an amplifier-subtraction stage (*U4*, R_a, R_b and R_c) has been added whose reference is adjustable by potentiometer (*Adjustable* V_{ref}). This stage, in addition to eliminating the DC value, allows additional amplification to increase the sensitivity of the system. In this case a 6.4 amplification has been taken which gives a total amplification of more than 320, large enough for our application.

For the *U2*, *U3* y *U4* we have used AD8625 IC with four OA.

The design of the Wien bridge oscillator has been made to guarantee a stability better than 2.5 %, which is required in (3) to obtain a resolution of 0.1 pF (3.2 mV LSB-ADC).

In order to validate the design, an analytical study of noise for the measurement circuit has been carried out. For this purpose, circuit in Fig. 3 has been split in four stages (Fig. 4 up), showing the considered noise sources.

Total rms noise has been evaluated using noise models for OAs, resistors and diodes [25], [26]. AD8627 (oscillator) and AD8625 (rectifier and offset suppression) have 17.5 nV/√Hz (e_n) spectral voltage noise density. AD8221 (IA) has 8 nV/√Hz (e_n) spectral voltage noise density, and 40 fA /√Hz (i_n) spectral current noise density. The spectral noise voltage density e_R is associated with the thermal noise of the resistors. For calculations, we have assumed that all the noise is Gaussian.

As shown in Fig. 4, the main spectral noise contributions come from both the IA stage and the offset-suppression stage (ZS), due to their relatively high gains (50.4 for the IA and 5.1 for the ZS). Due to the IA higher gain its noise contribution is the most important one. The IA amplifies input noise sources (the one coming from the oscillator as well as the noise of the De Sauty bridge and its own IA internal noise, all referred to the input) while the ZS stage amplifies the IA spectral output noise. Other noise contributions due to the rectifier and currents in OAs are negligible.

Figure 3b shows the main spectral contribution of IA noise sources.

Equation (4) gives e_{s1}, the spectral contribution due to the oscillator, assuming $R_o \sim R_x$ and $C_o \sim C_x$,

$$e_{s1} = \sqrt{2}\left(\frac{e_{so1}}{1+j\omega R_o C_o}\right) \tag{4}$$

Equation (5) gives e, the i_n contribution on Z_x and Z_o impedances ($R_x//C_x$ and $R_o//C_o$, respectively),

$$e = \sqrt{2}(Z_o i_n) \tag{5}$$

Equation (6) gives e_Z, the contribution due to the AI input impedances ($R_x//C_x$) and ($R_o//C_o$),

$$e_Z = \sqrt{2}e_o \tag{6}$$

where $e_o = \sqrt{KT/C_o}$.

Equation (7) gives the IA output spectral contribution,

$$e_{os2} = G\sqrt{e_{s1}^2 + e_n^2 + e^2 + e_z^2} \tag{7}$$

where G is the IA gain.

The total rms noise value is then obtained by square-summing the contribution of the spectral noise densities of the stages over the equivalent noise bandwidth of the low-pass filter $B \cong 1.57 f_c$, where f_c is the 1 Hz low-pass filter cut-off frequency. Considering the two main components (i.e. IA and ZS), we have evaluated e_{os4} to rise up to 2.3 mV/√ Hz. Taking into account $B \cong 1.57$ Hz, the estimated total rms noise is 2.8 mV, lower than the ADC LSB voltage value for the selected microcontroller (i.e. 3.2 mV).

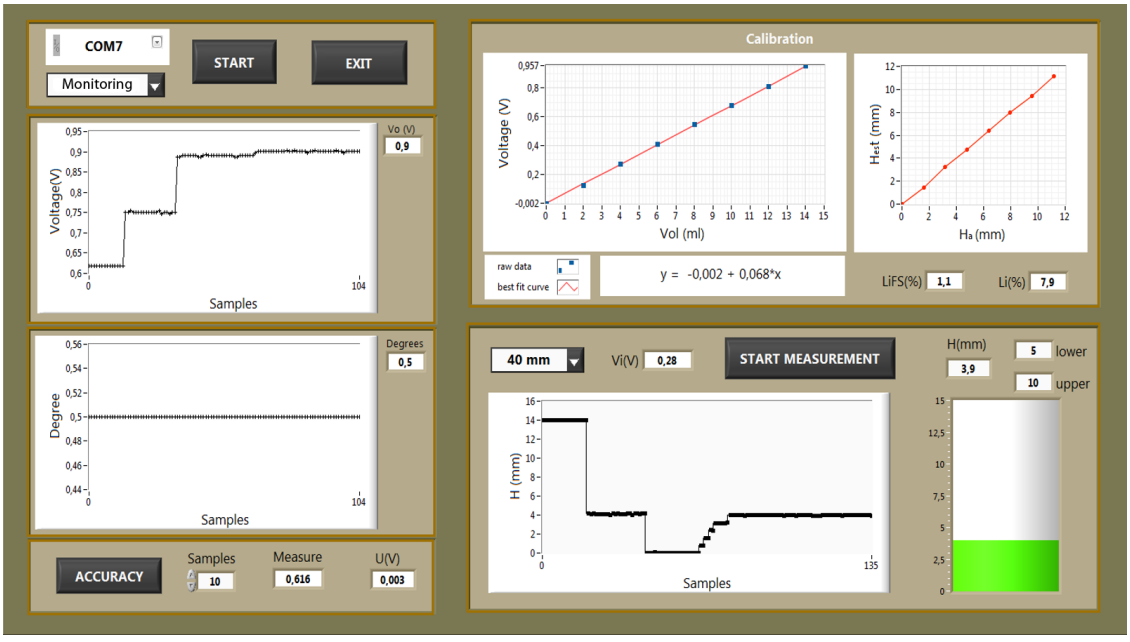

Fig. 5. User interface.

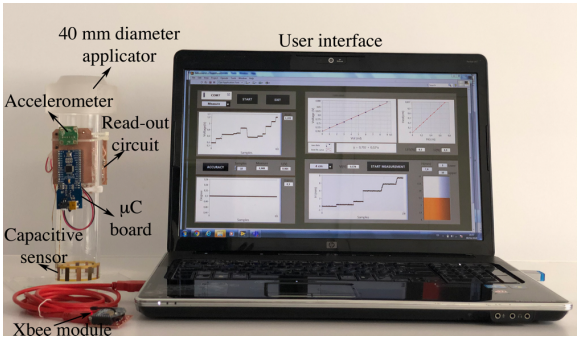

Fig. 6. Experimental set-up for the 40 mm diameter applicator.

The microcontroller acquires V_o and transmits it wirelessly to the computer (Fig. 3). Moreover, the tilting angle of the applicator is also measured by using the low-power accelerometer ADXL335 from Analog Devices and transmitted wirelessly to the computer. An Arduino FIO board based on the ATmega328P microcontroller (10 bits ADC, 3.2 mV LSB) is used together with two Xbee modules from Digi International that communicate through the Zigbee protocol.

C. Monitoring

In order to characterize the circuit and to automate the experimental tests, an application based on the LabVIEW software has been developed. Fig. 5 shows the user interface developed to perform repeatability tests. The application includes four functions:

- Monitoring (upper left): displays the acquired information (voltage V_o and tilting angle of the applicator). The time between each acquisition is less than 1 second.
- Measurement and uncertainty (lower left): make measurements of voltage V_o and tilting angle of the applicator. It shows the extended uncertainty (coverage factor $k = 2$).
- Calibration (upper right): shows the estimated characteristic curve and the independent linearity. Data is recorded in a file for further processing.
- Fluid level (lower right): graphically monitors the height of the fluid. A color code (green, orange, red) indicates the level of fluid present in the applicator (below the lower limit; between the preset alarm levels; above the upper limit).

III. Experimental Results

Figure 6 shows the set-up used for the test carried out using the 40 mm diameter applicator.

In order to characterize the circuit and obtain the estimated calibration curves (V_o in Fig. 3 vs height of fluid), experimental tests were carried out using water as fluid with a controlled temperature room between 17-22 ºC. Data are collected with the developed monitoring application. The tests were carried out for 0º and 45º tilting angles: 40 tests with the applicator 0º tilted and 40 tests with the applicator 45º tilted. Each test consists of 10 calibration processes (8 points were acquired to obtain one calibration process, each point corresponding to the average of 10 measurements). Three different observers have repeated these tests over a period of one month.

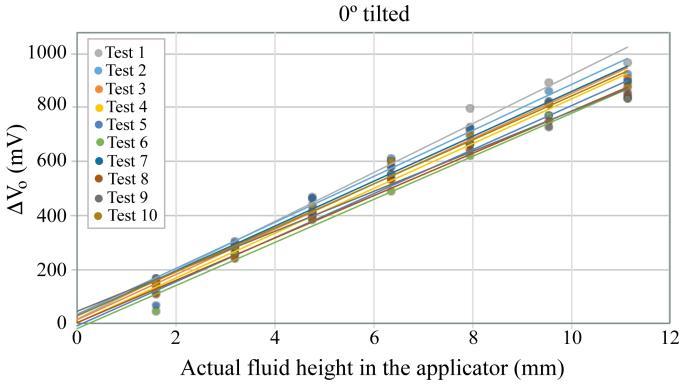

Fig. 7. Calibration curves for applicator 0º tilted. ΔV_o is the output voltage after suppression of zero condition.

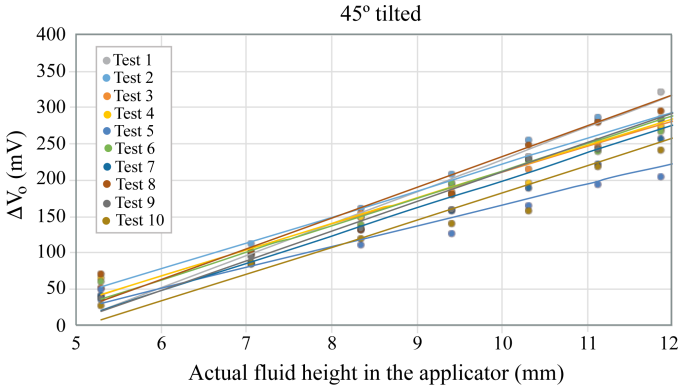

Fig. 8. Calibration curves for applicator 45º tilted. ΔV_o is the output voltage after suppression of zero condition.

Fig. 7 and Fig. 8 show calibration curves (one observer) in the region of the dynamic range (3-12 mm) for the applicator 0º and 45º tilted, fitting linear behavior ($R^2 > 0.99$ and 0.97 for 0º and 45º tilting angles, respectively). A variation of the zero condition (baseline drift) lower than 200 mV has been observed for each test, mainly due to the effect of the stray capacitance of the prototype. The output voltages shown in Fig. 7 and 8 correspond to values after baseline suppression (ΔV_o) of the considered test.

Calibration points in Fig. 7 correspond to 2 ml volume increments being equivalent to 1.6 mm increments. Likewise, calibration points in Fig. 8 correspond to volume increments of 0.5 ml being equivalent to height increments beginning from 5.3 mm down to 0.8 mm as water is added.

In agreement with Sanchis et al. [6], a slight fringing effect at both boundaries of the sensor (below 3 mm and above 12 mm) has been detected (not shown in Fig. 7 and Fig. 8).

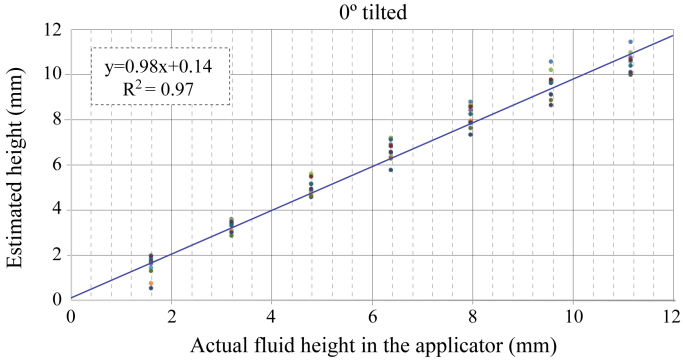

Fig. 9. Estimated height vs actual height of fluid for the obtained mean sensitivity when the applicator is 0º tilted.

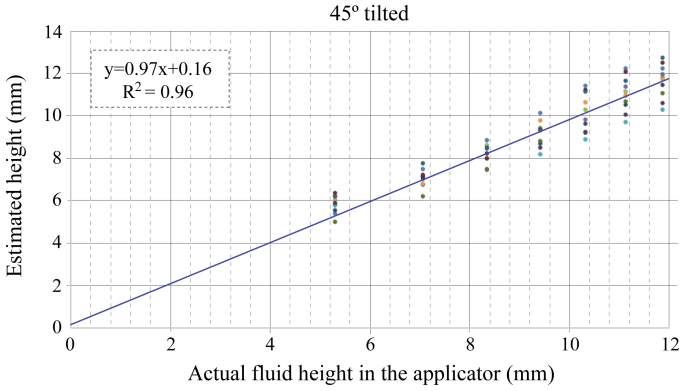

Fig. 10. Estimated height vs actual height of fluid for the obtained mean sensitivity when the applicator is 45º tilted.

A repeatability and reproducibility (R&R) one-way ANOVA study [27] has been carried out with the sensitivity data obtained during the calibration process (three observers). Table I summarizes the R&R results, where s_r and s_R are the repeatability and reproducibility standard deviation, respectively. Table II shows parameters and results of the calibration tests. A sensitivity of 85.5 ± 9.0 mV/mm for 0º tilting angle and 36.5 ± 9.8 mV/mm for 45º tilting angle has been obtained (coverage factor k=2 for both cases). Calibration curves show an independent linearity of 7.3 % and 11.4 % for 0º and 45º tilting angles, respectively.

From the sensitivity results obtained through the R&R analysis we have estimated the fluid height in the applicator.

TABLE I
ANOVA TEST RESULTS AND R&R ESTIMATORS

Tilting angle	p-value	s_r (mV/mm)	s_R (mV/mm)
0º	0.98	4.5	4.3
45º	0.56	4.9	4.8

TABLE II
MAIN CALIBRATION PARAMETERS

Tilting angle	Volume range (ml)	Height range (mm)	Sensibility (mV/mm)	Independent linearity (%)
0º	0.0-14.0	0.0-11.0	85.5 ± 9.0	7.3
45º	0.5-5.0	5.3-13.7	36.5 ± 9.8	11.4

TABLE III
LINEAR REGRESSION PARAMETERS (FIG. 9 AND FIG. 10)

Tilting angle	slope	intercept	R^2
0º	0.98 ± 0.13	0.14 ± 0.13	0.97
45º	0.97 ± 0.02	0.16 ± 0.18	0.96

Fig. 9 and Fig. 10 show the estimated height vs the actual height as well as the height errors for the worst-case calibration values. Maximum errors are ± 1 mm and ± 2 mm for the applicator 0º and 45º tilted, respectively.

Figures 9 and 10 show the correlation between the estimated height and the actual height in the applicator for a significant set of experimental measurements. In both cases, the actual height has been obtained numerically from the volume of fluid introduced while the estimated height has been obtained by dividing the output voltage corresponding to each of the measurements by the corresponding average value of the sensitivity, previously calculated using R&R analysis.

Linear regression parameters corresponding to Fig. 9 and Fig. 10 are given in Table III (fits have been done using a linear expression). Errors in parameters are compatible with those associated to experimental data.

For 0º tilted a ~2 mm height fluid detection is achieved well below the 5 mm height demanded by clinic while for 45º tilted is ~5 mm. It should be noted that for 45º tilted the fluid is not evenly distributed over the entire surface of the applicator but is located in the corner. Specifically, a fluid depth of 5 mm represents a volume as low as 0.5 ml, which occupies less than 10 % of the total surface of the applicator [6].

In what concerns the wireless power supply, accordingly to the fixed separation between the primary and secondary antenna (less than 5 mm) a current lower than 300 mA is obtained to charge SC. It takes approximately 20 min for the SC to charge up to the zener Z diode conduction (Fig. 2). Once the charging of SC is finished the primary antenna is removed. The SC takes approximately 80 min to discharge from 4.0 to 1.0 V. The voltage across the SC is not fully discharged to 0 V, as the boost regulator circuitry has an under-voltage threshold of around 0.95 V. Hence, once the input voltage drops below this limit, no power will be supplied to the measurement circuit.

IV. CONCLUSION

A read-out circuit to detect bleeding in IOERT applications has been presented. The circuit has been characterized in the worst-case clinical situation, being this the 40 mm diameter applicator, when it is tilted 0º and 45º. Thermal conditions are similar to the irradiation room (i.e. 20-24 ºC). A sensitivity of (86 ± 10) mV/mm has been obtained when the applicator is 0º tilted and (37 ± 9) mV/mm when the applicator is 45º tilted. The bleeding detector read-out circuit measures fluid levels between 0-12 mm with ± 1 mm error when the applicator is 0º tilted and ± 2 mm error when the applicator is 45º tilted.

A 2 mm height fluid detection is achieved for the 40 mm diameter applicator 0º tilted, well below the 5 mm height demanded by clinic. For 45º tilted we detect a fluid height of 5 mm. It should be noticed that in this extreme case the fluid is accumulated into the corner of the applicator and it is not

distributed to its central part. In particular, the 5 mm height limit represents a surface occupancy in the applicator lower than 10 %. This very small fraction could be considered acceptable from the clinical practice point of view.

A wireless power stage based on SC has been designed and tested achieving an autonomy around 80 min well above what is required by the clinic. SC charging time is around 20 min. The experimental results verify the usefulness of the implemented circuit to clearly guarantee the adequate detection of the maximum allowed level by clinic. The bleeding detector electronics described in this paper has linear sensitivity, low-cost, wireless low-power consumption being suitable for its future industrialization.

Future work will include embedding both sensor and electronics into the applicator as well as studies on clinical calibration and uses.

References

[1] E. C. Halperin, D. E. Wazer, L. W. Brady, and C. A. Perez, *Perez and Brady's principles and practice of radiation oncology*. 2013.

[2] H. L. Gunderson LL, Willett CG, Calvo FA, *Intraoperative Irradiation. Techniques and Results*, 2th ed. Springer, 2011.

[3] Calvo FA, "Intraoperative irradiation: Precision medicine for quality cancer control promotion," *Radiat. Oncol.*, vol. 12, no. 1, pp. 1–5, 2017, doi: 10.1186/s13014-017-0764-5.

[4] J. López-Tarjuelo, V. Morillo-Macías, A. Bouché-Babiloni, C. Ferrer-Albiach, and A. Santos-Serra, "Defining Action Levels for In Vivo Dosimetry in Intraoperative Electron Radiotherapy," *Technol. Cancer Res. Treat.*, vol. 15, no. 3, pp. 453–459, 2015, doi: 10.1177/1533034615588196.

[5] E. Sanchis *et al.*, "Detector for monitoring potential bleeding during electron intraoperative radiotherapy," *Phys. Medica*, vol. 57, no. July 2018, pp. 95–99, 2019, doi: 10.1016/j.ejmp.2018.12.010.

[6] E. Sanchis *et al.*, "Improving bleeding detector features for electron intraoperative radiotherapy," *Phys. Medica*, vol. 65, no. June, pp. 150–156, 2019, doi: 10.1016/j.ejmp.2019.08.015.

[7] A. Nevelsky, Z. Bernstein, R. Bar-Deroma, A. Kuten, and I. Orion, "Design and dosimetry characteristics of a commercial applicator system for intra-operative electron beam therapy utilizing ELEKTA Precise accelerator," *J. Appl. Clin. Med. Phys.*, vol. 11, no. 4, pp. 57–69, 2010, doi: 10.1120/jacmp.v11i4.3244.

[8] S. C. Bera, H. Mandal, S. Saha, and A. Dutta, "Study of a modified capacitance-type level transducer for any type of liquid," *IEEE Trans. Instrum. Meas.*, vol. 63, no. 3, pp. 641–649, 2014, doi: 10.1109/TIM.2013.2282194.

[9] C. A. Gong *et al.*, "Low-Cost Comb-Electrode Capacitive Sensing," vol. 16, no. 9, pp. 2896–2897, 2016.

[10] G. Barile *et al.*, "Linear Integrated Interface for Automatic Differential Capacitive Sensing," *Proceedings*, vol. 1, no. 4, p. 592, 2017, doi: 10.3390/proceedings1040592.

[11] R. T. Bento, R. W. O. Silva, L. A. Dias, A. Ferrus Filho, and A. J. C. Pitta, "Design, development and application of a real-time capacitive sensor for automatically measuring liquid level," *SN Appl. Sci.*, vol. 1, no. 7, pp. 1–8, 2019, doi: 10.1007/s42452-019-0770-3.

[12] S. F. Ali and N. Mandal, "Design and development of an electronic level transmitter using inter digital capacitor," *IEEE Sens. J.*, vol. 19, no. 13, pp. 5179–5185, 2019, doi: 10.1109/JSEN.2019.2903296.

[13] S. M. Huang, A. L. Stott, R. G. Green, and M. S. Beck, "Electronic transducers for industrial measurement of low value capacitances," *J. Phys. E.*, vol. 21, no. 3, pp. 242–250, Mar. 1988, doi: 10.1088/0022-3735/21/3/001.

[14] A. Elsaftawy, J. Potts, and W. Ahmed, "Oscillation Frequency LC-Based Sensor for Characterizing Two-Phase Flows in Energy Systems," *IEEE Sens. J.*, vol. 19, no. 1, pp. 65–77, 2019, doi: 10.1109/JSEN.2018.2876200.

[15] P. Vooka and B. George, "An Improved Capacitance-to-Digital Converter for Leaky Capacitive Sensors," *IEEE Sens. J.*, vol. 15, no. 11, pp. 6238–6247, Nov. 2015, doi: 10.1109/JSEN.2015.2454531.

[16] O. Lopez-Lapeña, E. Serrano-Finetti, and O. Casas, "Calibration-less direct capacitor-to-microcontroller interface," *Electron. Lett.*, vol. 52, no. 4, pp. 289–291, 2016, doi: 10.1049/el.2015.3706.

[17] E. Alnasser, "A Novel Fully Analog Signal Conditioning Circuit for Loss-Less Capacitive Sensor Estimation," *IEEE Sens. J.*, vol. 19, no. 18, pp. 8019–8026, 2019, doi: 10.1109/JSEN.2019.2917029.

[18] A. Ulla Khan, T. Islam, and J. Akhtar, "An Oscillator-Based Active Bridge Circuit for Interfacing Capacitive Sensors with Microcontroller Compatibility," *IEEE Trans. Instrum. Meas.*, vol. 65, no. 11, pp. 2560–2568, 2016, doi: 10.1109/TIM.2016.2581519.

[19] T. Islam, "Advanced Interfacing Techniques for the Capacitive Sensors," in *Smart Sensors, Measurement and Instrumentation*, 2017, pp. 73–109.

[20] J. Jeong, J. Xu, H. Jo, J. Li, and S. La, "Development of wireless sensor node hardware for large-area capacitive strain monitoring," 2019.

[21] S. C. Bera, J. K. Ray, and S. Chattopadhyay, "A low-cost noncontact capacitance-type level transducer for a conducting liquid," *IEEE Trans. Instrum. Meas.*, vol. 55, no. 3, pp. 778–786, 2006, doi: 10.1109/TIM.2006.873785.

[22] P. Mantenuto, A. De Marcellis, and G. Ferri, "Novel modified de-sauty autobalancing bridge-based analog interfaces for wide-range capacitive sensor applications," *IEEE Sens. J.*, vol. 14, no. 5, pp. 1664–1672, 2014, doi: 10.1109/JSEN.2014.2301296.

[23] A. P. Hu *et al.*, "Wireless Power Supply for ICP Devices With Hybrid Supercapacitor and Battery Storage," vol. 4, no. 1, pp. 273–279, 2016.

[24] N. A. Quadir, L. Albasha, M. Taghadosi, N. Qaddoumi, and B. Hatahet, "Low-Power Implanted Sensor for Orthodontic Bond Failure Diagnosis and Detection," vol. 18, no. 7, pp. 3003–3009, 2018.

[25] P. Lee, "Analog Devices Application Note, AN-940," *Analog Devices Appl. Note, AN-940*, pp. 1–12.

[26] Texas Instruments, "Noise Analysis in Operational Amplifier Circuits," *Digit. Signal Process. Solut. SLVA043A*, p. 87, 2007.

[27] L. E. S. (Eds. . Horst Czichos, Tetsuya Saito, *Springer Handbook of Metrology and Testing*, vol. 49, no. 0. 2011.